https://doi.org/10.5194/egusphere-2026-6868
Preprint. Discussion started: 12 November 2026
© Author(s) 2026. CC BY 4.0 License.

Brief communication: Impact of a bedrock–ice collapse on glacier dynamics: the 2026 Gyirong-Rasuwa disaster, Central Himalaya, Nepal

Ankit Pramanik[1], Mathieu Morlighem[2], Mohd. Farooq Azam[1,3]

[1] International Centre for Integrated Mountain Development (ICIMOD), Kathmandu, Nepal
[2] Department of Earth and Planetary Sciences, Dartmouth College, USA
[3] Department of Civil Engineering, Indian Institute of Technology Indore, India

Correspondence to: Ankit Pramanik (ankit.pramanik@icimod.org)

Abstract. On 26 August 2026, a massive collapse of bedrock and glacier ice from the north face of Langtang-Lirung, Nepal, triggered a catastrophic flash flood, leaving a steep, high-relief ice cliff. Two post-disaster scenarios are plausible: (1) continual small-scale break-off; and (2) creep over the relief, forming a hanging glacier prone to episodic, larger collapses. We test both with an ice-flow model. In both scenarios, ice velocity doubles immediately after the collapse and then gradually recovers. Continual break-off limits tensile-stress rise while hanging-glacier sustains tensile stress within the reported range of ice tensile strength, promoting crevassing and fracture, if not collapse.

1 Introduction

Incidents of glacier and bedrock–ice collapse have been observed in several regions worldwide in recent decades (Haeberli et al., 2004; Kääb et al., 2018; Shugar et al., 2021). Such events are expected to become more frequent with climate warming because of rapid changes in cryosphere, such as, receding of glaciers and thawing of permafrost (Azam et al., 2026). Many of these collapses have caused catastrophic disasters, with loss of lives, livelihoods, and infrastructure (Francese et al., 2025; Shugar et al., 2021), while many others likely went unreported because they were not associated with a disaster (Kääb et al., 2018).

On 26 August 2026, a mass of bedrock and overlying glacier ice (bedrock-ice collapse) broke away from the north face of the Langtang Lirung massif in Nepal, sending a sudden, destructive flash flood downstream that took thousands of lives and destroyed homes, land, livelihoods, and infrastructures (ICIMOD, 2026).

The collapse exposed a glacier ice cliff on steep relief, toward which the glacier will gradually advance post-disaster. The sudden loss of glacier terminus is expected to increase the flow velocity of the remnant glacier and deliver ice more rapidly to the cliff. Two outcomes are likely: the ice either breaks off continually in small chunks when it reaches the cliff, or the ice margin will creep gradually down the steep slope to form a hanging glacier. While the former is more probable, the latter cannot be ruled out.

Here, we investigate the consequences of the bedrock–ice collapse on the remnant glacier dynamics and model the effects of these two possible scenarios through prognostic experiments using the Ice-sheet and Sea-level System Model (ISSM).

https://doi.org/10.5194/egusphere-2026-6868
Preprint. Discussion started: 12 November 2026
© Author(s) 2026. CC BY 4.0 License.

2 Study area and data

The bedrock–ice collapse occurred at an unnamed glacier having RGI-id: 15.05732, situated on the north face of the Langtang Lirung massif in the Lhende Khola basin, Nepal (Fig, 1a-b). The glacier is ~2.5 km long and spans from 4700 m (terminus) to 5540 m in elevation. Its area was 2.35 km² before the collapse and 2.11 km² after (i.e., it lost 10% of its surface area) (Fig. 1c-f).

To conduct ice-dynamics experiments, we use the 2 m surface DEM derived from Pléiades satellite imagery (Berthier, 2026). The glacier mask is taken from the Randolph Glacier Inventory (RGI 7.0 Consortium, 2023) and modified to represent only the upper glacier, from which the bedrock–ice collapsed; it is further clipped to the upper section where the velocity and ice-thickness data are available (Millan et al., 2022). The mask of the collapsed area is derived from pre- and post-disaster Pleiades and Worldview satellite images, respectively (Berthier, 2026; Shean & Bhushan, 2026).

We use 2 m resolution post-disaster topography of the collapsed area, which was derived from optical stereo DEMs by Shean & Bhushan, 2026. To have complete coverage of the collapsed area, it was gap-filled with the 8 m resolution SAR stereo DEMs, prepared by Shean (2026).

In the absence of a surface mass balance (SMB) measurement for the northern side of the Langtang Lirung massif, we adopt the mass balance of Yala Glacier (Acharya & Kayastha, 2019; Stumm et al., 2021), which is on the southern side of the Langtang Lirung massif and has an elevation range comparable to that of our study glacier (Fig. S1). SMB is prescribed as a piecewise-linear function of surface elevation Z, using a clean-ice gradient above the equilibrium-line altitude (ELA) and a debris-shielded ablation gradient below the debris limit Z_d, converted directly to ice-equivalent units:

$$SMB(Z) = \frac{\rho_w}{\rho_{ice}} \begin{cases} \min(C_{acc}(Z - Z_{ELA}), A_{max}) & Z > Z_{ELA} \\ -C_{abl}(Z_{ELA} - Z) & Z_d < Z \leq Z_{ELA} \\ \max(C_{abl}(Z_{ELA} - Z_d) - f_d C_{abl}(Z_d - Z), A_{min}) & Z \leq Z_d \end{cases}$$

where ρ_w, ρ_{ice} are the freshwater and ice densities. The parameter values used are provided in Table S1.

We use ice thickness and velocity data from Millan et al. (2022). Ice thickness is ~20 m at the snout, ~80 m at the relief, which is ~800 m from the snout, and reaches ~185 m at the centre of the glacier (Fig. 1d). Surface velocity is highest (~90 m yr^{-1}) at the steep frontal slope (~33°) and decreases upstream where the bed flattens (~8°) (Fig. S1).

3 Methods

3.1 Ice-flow model

We use the ice-flow model ISSM (Larour et al., 2012) with the shallow-shelf approximation (SSA) to investigate glacier dynamics after the collapse. As we focus on the glacier's immediate response to the collapse close to the terminus where ice velocity is primarily dictated by sliding, the SSA offers a fast and reliable basis for simulation (MacAyeal, 1989). Anisotropic mesh adaptation produced a finite-element mesh of 15–150 m resolution, refined first on bed-topography gradients and then on gradients in satellite-derived ice-flow velocities (Millan et al., 2022).

https://doi.org/10.5194/egusphere-2026-6868
Preprint. Discussion started: 12 November 2026
© Author(s) 2026. CC BY 4.0 License.

Observed surface velocities from Millan et al. (2022) are used to invert for the basal friction coefficient via a Budd sliding law (Budd et al., 1979) using the glacier geometry before the collapse. Observed and modelled velocities, their difference, and the inferred basal friction coefficient are shown in Fig. S2.

3.2 Experiments

We first run the model for one year with the initial (pre-collapse) geometry. We then conduct two experiments in which bedrock and ice are removed from the collapsed area to represent the two plausible scenarios:

1. **Break-off (Fixed front):** the glacier front is held fixed, so ice is lost immediately once it crosses the cliff.
2. **Hanging (Moving front):** the glacier advances past the cliff and creeps along the bedrock, forming a hanging glacier.

Both these scenarios are simulated for 2 years. These experiments allow us to examine how the glacier responds under immediate versus delayed break-off and to assess the risk of future hazards from the same area.

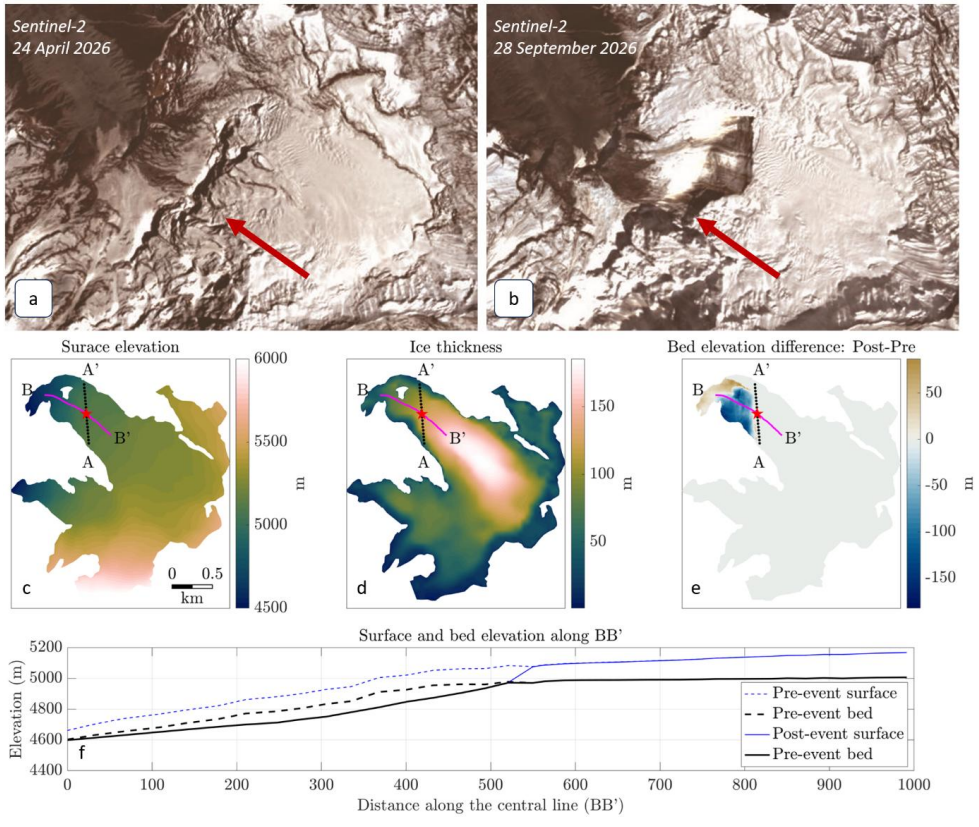


Fig. 1: Sentinel-2 satellite images of the glacier (a) before, and (b) after the bedrock-ice collapse. Red arrows show the ice flow direction. (c) Surface DEM, (d) Ice thickness, and (e) Bed elevation difference before and after the collapse. Non-zero elevation difference zone in (e) indicates the bedrock-ice collapse area. Post-collapse moderate increase in bed elevation at the lower part of glacier is likely due to the removal of ice followed by deposition of debris. Black

https://doi.org/10.5194/egusphere-2026-6868
Preprint. Discussion started: 12 November 2026
© Author(s) 2026. CC BY 4.0 License.

circles (AA') are the points on the transect across the glacier where velocity, mass flux and tensile stress are calculated. The red star is a point where time series results are shown. BB' is the length of the longitudinal profile along the central line of the glacier starting from the pre-collapse glacier snout. (f) The central line (BB') profile of surface and bed before and after collapse.

4 Results

4.1 Velocity and mass flux

Within one day of the collapse, ice velocity at the glacier front (~0.5 km^2 area) increases by >30 m/yr; around 60% increase in mean velocity from 50 to 82 m yr^{-1}. The largest increase occurs at the mid-point of the transect, where ice is thickest, and more than doubles relative to the pre-event velocity (Fig. 2a-b).
Velocity thereafter evolves differently in the two scenarios: in the break-off experiment, the mean velocity recovers gradually from 82 m yr^{-1} to 60 m yr^{-1} by the end of year 2, whereas in the hanging experiment the mean velocity continues to rise (from 82 to 89 m yr^{-1}) until day 60 before declining gradually (Fig. 2c). This acceleration draws down ice mass, exponentially thinning the mean ice thickness across the glacier front (Fig. 2d). The thinning rate is sharper in the hanging scenario and later feeds back on velocity, making it equal to break-off by day 600.

These changes in velocity and thickness alter the mass flux across the glacier, which increases immediately after the event, doubling the pre-event value at the mid-transect (Fig. 2e). The hanging experiment shows an initial rise in mass flux that remains elevated until day 200, after which it converges toward the break-off value and remains comparable until day 500 (Fig. 2e). Beyond day 500, the hanging mass flux lags the break-off mass flux, reflecting the competing interplay between velocity and ice thickness post-collapse. Therefore, the hanging scenario produces an abrupt initial mass loss, whereas the break-off scenario produces a gradual but sustained mass loss. Net mass outflow beyond the edge of the relief (AA' line) after two years is 2.52 Gt and 2.59 Gt for the break-off and hanging scenarios, respectively, reflecting equivalent total mass loss up to 2 years occurring through two different pathways.

4.2 Stress

The rapid post-collapse ice velocity increase in turn perturbs the stress response of the glacier near the cliff. Tensile stress rises abruptly immediately after the collapse (from ~140 kPa to ~250 kPa) in both scenarios. It then decreases gradually in the break-off experiment, whereas in the hanging experiment it increases further before declining. As ice is shed off the cliff continuously, the stress response remains contained in the break-off scenario. In the hanging experiment, the first principal stress (tensile) shows frequent fluctuations in peak magnitude before stabilizing at ~190 kPa after 500 days (Fig. 3a); the maximum tensile stress at the ice cliff reaches 296 kPa on day 111 (Fig. 3b). The hanging arm along the steep relief imposes an additional pull that keeps tensile stress elevated near the cliff even after stabilization (Fig. 3c-e), relative to the break-off scenario. At its maximum extent, an area of ~0.5 km^2 adjacent to the cliff experiences stress above 200 kPa. These magnitudes fall within the range of reported ice tensile strength (Brondex et al., 2026; Grinsted et al., 2024; Vaughan, 1993), leaving the hanging arm susceptible to collapse under external triggers such as earthquakes, and promoting fracture and crevassing if not outright collapse.

https://doi.org/10.5194/egusphere-2026-6868
Preprint. Discussion started: 12 November 2026
© Author(s) 2026. CC BY 4.0 License.

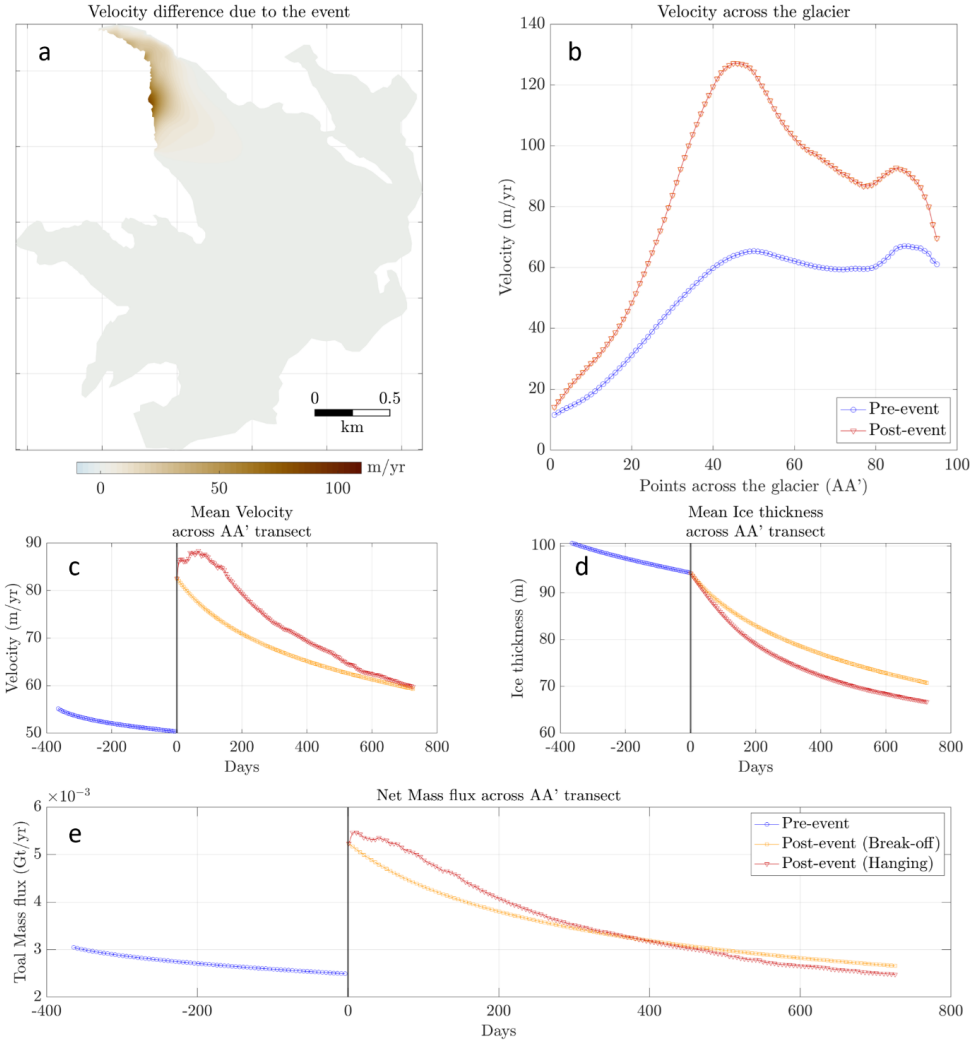


Fig. 2: (a) Velocity difference between before and immediately after the bedrock-ice collapse. (b) Pre- and post-collapse velocity after one day of the collapse across the AA' transect of the glacier (Fig. 1). Evolution of mean (c) velocity and (d) ice thickness. The mean is calculated for all points of the AA' transect. (f) Total mass flux across AA' over time. All subplots show results of pre-event and post-event (Break-off and Hanging) experiments.

https://doi.org/10.5194/egusphere-2026-6868
Preprint. Discussion started: 12 November 2026
© Author(s) 2026. CC BY 4.0 License.

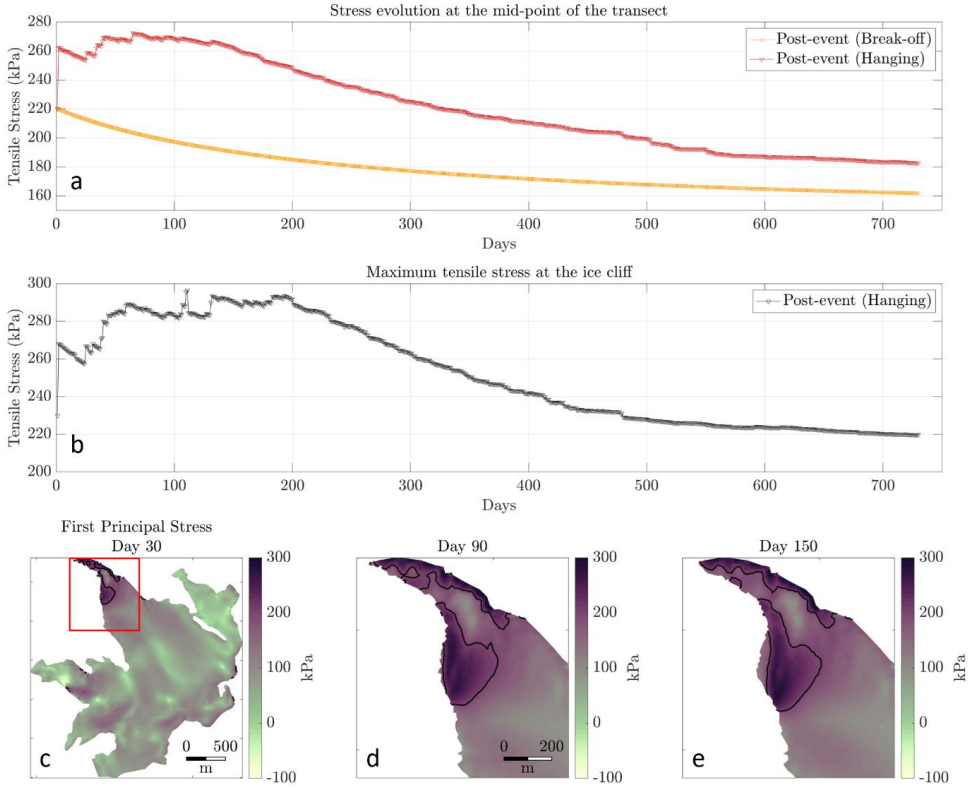


Fig. 3: (a) Principal tensile stress change at the mid-point of the AA' transect for Break-off and Hanging scenarios. (b) Maximum value of tensile stress at the ice cliff area for the Hanging scenario. The maximum value for the Break-off scenario follows the mid-point value of the transect and is therefore not shown here. (c-e) Snapshots of the first principal stress field (positive when tensile) near the collapse area in 60 days interval for the Hanging experiment. The contour indicates the zone above 200 kPa tensile stress.

5 Discussion

Frontal ice buttresses the ice immediately upstream, maintaining an equilibrium velocity across the glacier that is set primarily by bed slope and ice thickness. The sudden loss of ice and bedrock removes this support, and the remaining ice begins to flow faster, accelerating and thinning until a new equilibrium is reached through sliding and deformation. Satellite images captured in different intervals after the event show rapid movement of glacier front (Slide 4-5, Nepal - Tibet Border Flood 2026 | Cesium Stories), consistent with our simulations.

As the ice accelerates, it reaches the newly formed cliff, where the bed is steep. There, it either breaks off or creeps gradually down the slope. In the initial days, high velocity and stress make break-off more probable. If the ice breaks continually in small chunks, flow remains elevated but steady over time, declining only over the long term as ice thickness decreases. Continual break-off sustains high frontal velocity, and the glacier loses mass faster than usual through dynamic thinning. Sustained high velocity may also gradually deform the bed, depending on the bedrock geology.

https://doi.org/10.5194/egusphere-2026-6868
Preprint. Discussion started: 12 November 2026
© Author(s) 2026. CC BY 4.0 License.

As the front slows and thins after 200 days, however, break-off becomes less likely and creep along the slope more likely, potentially forming a hanging glacier tongue that remains susceptible to episodic collapse. The modelled stress over 0.5 km^2 behind the collapsed front falls within reported ice tensile strength range of 158–300 kPa (Grinsted et al., 2024; Vaughan, 1993) and exceeds the crevasse initiation range of 100–130 kPa (Brondex et al., 2026). Given the steep relief, such stresses will very likely produce fractures and crevasses, as seen in icefalls, where the ice does not break off completely.

There is a further possibility of ice-cliff backwasting as observed after the Marmolada glacier collapse (Gusmeroli et al., 2026). Our study glacier, however, faces north, limiting the backwasting rate compared to south-facing glaciers (Sato et al., 2025). Further to that, the event occurred toward the end of the summer, when the energy availability for backwasting is lower. Therefore, the glacier is expected to undergo immediate downslope motion rather than backwasting, unlike the Marmolada glacier.

Uncertainty

The ice-thickness estimates (Millan et al., 2022) carry uncertainty that propagates into our results, and the observed velocities likewise carry uncertainty that affects the basal friction inversion and may depart from reality. For the post-event simulations, we applied the pre-event friction coefficient to the collapsed area. Because the collapse altered the topography, the actual post-event friction is likely different, which adds uncertainty to the hanging-glacier scenario results. A further limitation is the absence of an explicit representation of effective pressure, which influences sliding. Rapid changes in glacier velocity may alter the existing subglacial drainage structure and facilitate distributed drainage affecting the effective pressure. All of these affect the magnitude of our results but not the direction of change, which is our focus here.

Implications

Sustained high velocities, dynamic thinning and elevated tensile stresses, raise the risk of collapse of the hanging ice mass under external triggers: earthquakes, to which this region is highly prone, landslides from adjacent slopes, and extreme precipitation, all recurrent in this part of the world. Under these conditions, the threat of a further, similar disaster persists. Its severity depends on the volume of detached ice and on the now-greater post-collapse elevation difference.

This threat is not confined to a single site. The total number of hanging glaciers in the Hindu Kush Himalaya remains unreported, but 219 have been documented in the Alaknanda Basin of the Garhwal Himalaya alone (Krishnan et al., 2026). Across the region, hanging glaciers are subject to extreme temperature and precipitation under rapid climate change; these changes, combined with a tectonically active and high-relief mountain setting, make many of them vulnerable to partial collapse. We show that such a collapse not only generates downstream hazards but also perturbs glacier dynamics: it raises ice velocity, which may remain elevated for years until a new equilibrium is reached and draws down more mass from upstream, thinning the glacier and accelerating mass loss. A glacier collapse might therefore accelerate overall glacier mass loss.

While such collapses are difficult to prevent, they may be predicted. With the ice cliff exposed, the ice thickness at the site can be measured directly and used to validate ice-thickness modelling across the Himalaya (e.g., Millan et al., 2022). In that regard, this glacier could serve as a laboratory for understanding the dynamics of

https://doi.org/10.5194/egusphere-2026-6868
Preprint. Discussion started: 12 November 2026
© Author(s) 2026. CC BY 4.0 License.

hanging glaciers. A combination of satellite, seismic and on-ground observations is needed to anticipate future events, which is crucial for preventing future disasters.

6 Conclusions

The bedrock–ice collapse from the north face of Langtang Lirung massif exposed an ice cliff on steep relief, toward which the ice will gradually advance, leading either to continual break-off or to the formation of a hanging glacier. We find that the sudden collapse accelerates the glacier, producing a twofold increase in ice mass outflow, which is consistent with the observation.

We make the following predictions that will likely take place over time:

1. In the case of hanging-glacier formation, the ice velocity and mass flux will remain higher for one year compared with the continual break-off scenario, posing the threat of future hazard.
2. In the case of continual break-off, ice velocity and mass flux become higher than in the hanging-glacier scenario, leading to faster mass loss of the glacier.
3. If a hanging glacier forms, stress remains elevated and within the range of ice tensile strength, which will facilitate formation of fractures and crevasses, if not immediate collapse.
4. These fractures and crevasses would weaken the ice, leaving it susceptible to future collapse.

Our findings indicate the likely post-disaster response. Further study should incorporate ground observations of post-disaster glacier velocity, and DEM differencing to constrain the magnitude of change more robustly. Thus, active monitoring of this glacier will help not only in predicting future collapse but also in understanding the dynamics of hanging glaciers and the subsequent mass loss due to such events.

Code and data availability

ISSM is freely available at https://github.com/ISSMteam/ISSM. All the codes related to model simulations will be made available on GitHub upon publication. All the output data will be made publicly available upon publication of the paper.

Supplement

Author contributions

AP conceptualized the study with MM and MFA. AP set up the model, conducted the simulations, analysed the results and wrote the manuscript. MM helped in basal friction inversion. All authors participated in discussing results and reviewing the manuscript.

Acknowledgements

We thank Felipe Ugalde (University of Chile) for providing the initial shapefile of the glacier and bedrock-ice collapsed area, Etienne Berthier (CNRS, LEGOS, France) for preparing the pre-event glacier DEM, David

https://doi.org/10.5194/egusphere-2026-6868
Preprint. Discussion started: 12 November 2026
© Author(s) 2026. CC BY 4.0 License.

Shean (University of Washington, USA) for the post-event DEM, and Rashed Uz Zzaman (ICIMOD) for assistance with the QGIS mapping. We are grateful for all those researchers who put their initial results on different aspects of this disaster on public platforms, which gave us a detailed understanding of the disaster and motivated this work. We thank Sarah Greenwood (Stockholm University, Sweden) for reviewing the manuscript, and Dr. Qianggong Zhang, Head of the Climate and Environmental Risks Strategic Group, ICIMOD, and Dr. Pema Gyamtsho, Director General of ICIMOD, for their support.

References

Acharya, A., & Kayastha, R. B. (2019). Mass and Energy Balance Estimation of Yala Glacier (2011–2017), Langtang Valley, Nepal. *Water*, *11*(1), 6. https://doi.org/10.3390/w11010006

Azam, Mohd. F., Thakur, S. K., Muhammad, S., Kaushik, H., Sattar, A., & Sanyal, S. (2026). Cryosphere hazards under weather and climate extremes in the Hindu Kush Himalaya: The cryosphere hazard interaction pathways (CHiP) framework. *Progress in Disaster Science*, *32*, 100738. https://doi.org/10.1016/j.pdisas.2026.100738

Berthier, E. (2026). *13 October 2019 Pléiades (CNES) pre-event Digital Elevation Models (DEMs) for the rock-ice avalanche source area of the August 2026 Trishuli catastrophic flood.* [Data set]. https://doi.org/10.5281/zenodo.22147118

Brondex, J., Gagliardini, O., Gilbert, A., & Thibert, E. (2026). How to model crevasse initiation? Lessons from the artificial drainage of a water-filled cavity on the Tête Rousse Glacier (Mont Blanc range, France). *The Cryosphere*, *20*(3), 1655–1677. https://doi.org/10.5194/tc-20-1655-2026

Budd, W. F., Keage, P. L., & Blundy, N. A. (1979). Empirical Studies of Ice Sliding. *Journal of Glaciology*, *23*(89), 157–170. Cambridge Core. https://doi.org/10.3189/S0022143000029804

Francese, R. G., Valentino, R., Haeberli, W., Bondesan, A., Giorgi, M., Picotti, S., Pettenati, F., Sandron, D., Ramponi, G., & Valt, M. (2025). Failure of Marmolada Glacier (Dolomites, Italy) in 2022: Data-based back analysis of possible collapse mechanisms. *Nat. Hazards Earth Syst. Sci.*, *25*(9), 3027–3053. https://doi.org/10.5194/nhess-25-3027-2025

Grinsted, A., Rathmann, N. M., Mottram, R., Solgaard, A. M., Mathiesen, J., & Hvidberg, C. S. (2024). Failure strength of glacier ice inferred from Greenland crevasses. *The Cryosphere*, *18*(4), 1947–1957. https://doi.org/10.5194/tc-18-1947-2024

Gusmeroli, A., Carlà, T., Leva, D., Rivolta, C., Villa, F., & Casagli, N. (2026). Post-Collapse Ice Cliff Backwasting at the Marmolada Glacier Observed by Terrestrial Radar Interferometry. *Journal of Geophysical Research: Earth Surface*, *131*(3), e2025JF008367. https://doi.org/10.1029/2025JF008367

Haeberli, W., Huggel, C., Kääb, A., Zgraggen-Oswald, S., Polkvoj, A., Galushkin, I., Zotikov, I., & Osokin, N. (2004). The Kolka-Karmadon rock/ice slide of 20 September 2002: An extraordinary event of historical dimensions in North Ossetia, Russian Caucasus. *Journal of Glaciology*, *50*(171), 533–546. Cambridge Core. https://doi.org/10.3189/172756504781829710

ICIMOD. (2026). *Understanding the Gyirong–Rasuwa disaster of 26 August 2026: A preliminary synthesis*. International Centre for Integrated Mountain Development (ICIMOD). https://doi.org/https://doi.org/10.53055/ICIMOD.1150

https://doi.org/10.5194/egusphere-2026-6868
Preprint. Discussion started: 12 November 2026
© Author(s) 2026. CC BY 4.0 License.



Kääb, A., Leinss, S., Gilbert, A., Bühler, Y., Gascoin, S., Evans, S. G., Bartelt, P., Berthier, E., Brun, F., Chao, W.-A., Farinotti, D., Gimbert, F., Guo, W., Huggel, C., Kargel, J. S., Leonard, G. J., Tian, L., Treichler, D., & Yao, T. (2018). Massive collapse of two glaciers in western Tibet in 2016 after surge-like instability. *Nature Geoscience*, *11*(2), 114–120. https://doi.org/10.1038/s41561-017-0039-7

Krishnan, N., Sattar, A., Kulkarni, A. V., & Negi, H. S. (2026). Basin-scale inventory and exposure assessment of hanging glaciers, Central Himalaya. *Npj Natural Hazards*, *3*(1), 44. https://doi.org/10.1038/s44304-026-00205-8

Larour, E., Seroussi, H., Morlighem, M., & Rignot, E. (2012). Continental scale, high order, high spatial resolution, ice sheet modeling using the Ice Sheet System Model (ISSM). *Journal of Geophysical Research: Earth Surface*, *117*(F1). https://doi.org/10.1029/2011JF002140

MacAyeal, D. R. (1989). Large-scale ice flow over a viscous basal sediment: Theory and application to ice stream B, Antarctica. *Journal of Geophysical Research: Solid Earth*, *94*(B4), 4071–4087. https://doi.org/10.1029/JB094iB04p04071

Millan, R., Mouginot, J., Rabatel, A., & Morlighem, M. (2022). Ice velocity and thickness of the world's glaciers. *Nature Geoscience*, *15*(2), 124–129. https://doi.org/10.1038/s41561-021-00885-z

RGI 7.0 Consortium. (2023). *Randolph Glacier Inventory—A Dataset of Global Glacier Outlines, Version 7.0.* (Version 7.0) [Data set]. NSIDC. https://doi.org/10.5067/f6jmovy5navz

Sato, Y., Buri, P., Kneib, M., Miles, E. S., Sunako, S., Gurung, T. R., Sakai, A., Pellicciotti, F., & Fujita, K. (2025). Modelling seasonal fluctuations and aspect characteristics of ice-cliff melt on the debris-covered Trakarding Glacier, Rolwaling Valley, Nepal Himalaya. *Journal of Glaciology*, *71*, e33. Cambridge Core. https://doi.org/10.1017/jog.2025.17

Shean, D. (2026). *Post-event SAR stereo DEMs (Umbra) for the 2026-08-26 Rasuwa (Langtang Lirung) ice-rock avalanche, Nepal (Version v1.0)* [Data set]. https://doi.org/10.5281/zenodo.22842744

Shean, D., & Bhushan, S. (2026). *Post-event optical stereo DEMs (WorldView-2, WorldView Legion 2/3, WorldView-3) for the 2026-08-26 Rasuwa (Langtang Lirung) ice-rock avalanche, Nepal (v1.0)* [Data set]. https://doi.org/10.5281/zenodo.22842746

Shugar, D. H., Jacquemart, M., Shean, D., Bhushan, S., Upadhyay, K., Sattar, A., Schwanghart, W., McBride, S., de Vries, M. V. W., Mergili, M., Emmer, A., Deschamps-Berger, C., McDonnell, M., Bhambri, R., Allen, S., Berthier, E., Carrivick, J. L., Clague, J. J., Dokukin, M., … Westoby, M. J. (2021). A massive rock and ice avalanche caused the 2021 disaster at Chamoli, Indian Himalaya. *Science*, *373*(6552), 300–306. https://doi.org/10.1126/science.abh4455

Stumm, D., Joshi, S. P., Gurung, T. R., & Silwal, G. (2021). Mass balances of Yala and Rikha Samba glaciers, Nepal, from 2000 to 2017. *Earth Syst. Sci. Data*, *13*(8), 3791–3818. https://doi.org/10.5194/essd-13-3791-2021

Vaughan, D. G. (1993). Relating the occurrence of crevasses to surface strain rates. *Journal of Glaciology*, *39*(132), 255–266. Cambridge Core. https://doi.org/10.3189/S0022143000015926